Fabrication of superhydrophobic metallic porous surfaces via CO_2 and water processing

Anagnostopoulos, Argyrios; Nikulin, Artem; Knauer, Sandra; Bondarchuk, Oleksandr; Rivero, Maria Elena Navarro; Lu, Tiejun; Karkantonis, Themistoklis; Barrio, Elena Palomo del; Chorążewski, Mirosław A.; Li, Yongliang; Ding, Yulong; Meloni, Simone; Grosu, Yaroslav

DOI:
10.1016/j.apsusc.2023.157546

Document Version
Publisher's PDF, also known as Version of record

Citation for published version (Harvard):
Anagnostopoulos, A, Nikulin, A, Knauer, S, Bondarchuk, O, Rivero, MEN, Lu, T, Karkantonis, T, Barrio, EPD, Chorążewski, MA, Li, Y, Ding, Y, Meloni, S & Grosu, Y 2023, 'Fabrication of superhydrophobic metallic porous surfaces *via* CO_2 and water processing', *Applied Surface Science*, vol. 632, 157546. https://doi.org/10.1016/j.apsusc.2023.157546

Applied Surface Science 632 (2023) 157546

Contents lists available at ScienceDirect

Applied Surface Science

journal homepage: www.elsevier.com/locate/apsusc

Full Length Article

Fabrication of superhydrophobic metallic porous surfaces *via* CO_2 and water processing

Argyrios Anagnostopoulos [a,b], Artem Nikulin [c,*], Sandra Knauer [d], Oleksandr Bondarchuk [e], Maria Elena Navarro Rivero [a], Tiejun Lu [a], Themistoklis Karkantonis [f], Elena Palomo del Barrio [c,g], Mirosław A. Chorążewski [b], Yongliang Li [a], Yulong Ding [a], Simone Meloni [h,*], Yaroslav Grosu [b,c,*]

[a] *BCES Birmingham Centre of Energy Storage & School of Chemical Engineering, University of Birmingham, Birmingham B15 2TT, the United Kingdom of Great Britain and Northern Ireland*
[b] *Institute of Chemistry, University of Silesia in Katowice, Szkolna 9, 40-006 Katowice, Poland*
[c] *Centre for Cooperative Research on Alternative Energies (CIC energiGUNE), Basque Research and Technology Alliance (BRTA), Alava Technology Park, Albert Einstein 48, 01510 Vitoria-Gasteiz, Spain*
[d] *Eurotechnica GmbH, Bargteheide, Germany*
[e] *International Iberian Nanotechnology Laboratory, Av. Mestre José Veiga, s/n, 4715-330, Braga, Portugal*
[f] *Department of Mechanical Engineering, School of Engineering, University of Birmingham, Birmingham B15 2TT, the United Kingdom of Great Britain and Northern Ireland*
[g] *Ikerbasque – Basque Foundation for Science, Plaza Euskadi 5, 48009 Bilbao, Spain*
[h] *Dipartimento di Scienze Chimiche, Farmaceutiche ed Agrarie (DOCPAS), Università degli Studi di Ferrara (Unife), Via Luigi Borsari 46, I-44121, Ferrara, Italy*

A R T I C L E I N F O

Keywords:
Superhydrophobic surface
CO_2 hydrogenation
Hierarchical Porosity
Copper
Supercritical CO_2

A B S T R A C T

Superhydrophobic surfaces are of paramount importance for a great number of applications ranging from heat transfer to medicine. However, their mass production is challenging from environmental and scaling points of views. This work proposes a simple, scalable, production method for superhydrophobic surfaces and porous materials. In particular, highly hydrophobic CH_2/CH_3-grafted copper is achieved *via* exposure to a high-pressure supercritical $CO_2 + H_2O$ environment. The hydrophobicity was further reinforced by using hierarchical macro-nanoporous copper prepared by a simple templating-annealing method reaching a water contact angle of ~ 150°. The grafting is found to be durable in terms of ageing, abrasion and water impact. The superhydrophobic porous material is successfully used to separate oil emulsions from water. Molecular dynamics simulations are employed to investigate the underlying superhydrophobicity mechanisms further. We hypothesise that the obtained grafting results from a CO_2 hydrogenation reaction. The proposed approach may pave the way for the mass use of superhydrophobic surfaces and porous materials for anti-corrosion, anti-icing, separation, batteries, sensors, electronic materials, etc.

1. Introduction

Water-repelling behaviour is present across the natural habitat. Natural surfaces, such as the lotus leaf and rose petal, have inspired researchers to fabricate highly water-repellent surfaces [1]. Such surfaces exhibit very high contact angles (>151°) and have thus been coined as super- (or ultra-) hydrophobic [2]. Their popularity is ever-increasing in various fields, predominantly anti-corrosion [3], drag reduction [4], anti-icing [5], oil – water separation [6–9], anti-fogging [10], self-cleaning [11], anti-fouling [12], anti-bacterial [13], micro-droplet manipulation [14], stimulus-responsive surfaces [15] and shape memory materials [16]. Recent progress in underwater and flexible electronics, automotive, advanced textiles, high-end footwear, and food packaging industry sectors are key growth drivers for the super-hydrophobic coating market. An analytical report published by Mordor Intelligence (2021) estimated the current superhydrophobic coating market cap at 17 million USD with an expected compound annual growth rate (CAGR) of 25.2% in the 2022–2027 period [17].

* Corresponding authors.
E-mail addresses: anikulin@cicenergigune.com (A. Nikulin), simone.meloni@unife.it (S. Meloni), ygrosu@cicenergigune.com (Y. Grosu).

https://doi.org/10.1016/j.apsusc.2023.157546
Received 3 April 2023; Received in revised form 12 May 2023; Accepted 15 May 2023
Available online 20 May 2023

Superhydrophobicity is a physio-chemical phenomenon [18]. A combination of surface architecture (micro-nano patterning) and surface chemistry (low surface energy finishing) is required to generate a water-repellent material [19]. In fact, its physical aspect can be easily explained through the Cassie-Baxter and Wenzel models that prove the dependence of wettability on surface roughness [19]. Its chemical aspect has also been confirmed, for example, in the case of the lotus leaf, by identifying nubs covered with waxy nanocrystals [20]. In this context, the first requirement of a superhydrophobic surface is roughness, ideally multiscale [21]. The second is a low surface energy coating. There are several methods to shape the morphology of a metal surface and tune its hydrophobicity. These are wet methods, plasma methods, anodic oxidation, gas phase, and laser etching methods [22–23]. Surface energy is then typically reduced *via* the deposition of a low surface energy coating [24]. These are deposited through dry methods, most commonly chemical vapour deposition (CVD) and plasma polymerisation, or wet processes, such as immersion or spin coating.

Inspired by the lotus and petal effects, Li et al. fabricated copper surfaces with two distinct microstructures via polishing, sandblasting, and laser texturing. Both patterns exhibited a considerably delayed icing effect relative to the untreated copper surface [25]. Yamamoto et al. recently fabricated a superhydrophobic Cu metal nanowire surface through anodising in a KOH electrolyte, hydrogen reduction at an elevated temperature, and application of a toluene stearic acid wet coating. The result was a high thermal conductivity surface with good anti-fogging properties [26]. Multiscale copper textured surfaces were developed, by Mousavi and Pitchmunani, via low power short time electrodeposition. Following functionalisation (stearic acid), the surfaces achieved superhydrophobicity, which improved their corrosion inhibition efficiency by 99%, even at very low pH environments [27]. Yin et al. fabricated a superhydrophobic copper hydroxide-coated mesh through a facile spraying and surface modification approach, which was used for water–oil separation with an excellent efficiency>99% [28].

Chemical methods have minimal equipment requirements, low cost, and favourable conditions in large-scale production and are, therefore, the preferred route to superhydrophobic surface production. Wet chemical etching is a promising alternative, with projected low costs and easy scalability. However, most of these methods require a series of reagents, which are often hazardous, and have a limited range of applicable materials. In contrast, dry subtractive processes have a good range, and are very effective but have to overcome scaling limitations.

A superhydrophobic surface fabrication technology should be low-cost and easily scalable, with a minimal environmental footprint to be realistically applicable. To this end, in this work, a straightforward fabrication process for superhydrophobic copper is presented. The process involves a facile templating protocol followed by chemical modification using supercritical CO_2 (sCO_2) and water. Supercritical CO_2 has been widely explored in superhydrophobic coating formation mostly through the rapid expansion of the supercritical solutions method (RESS) or as an antisolvent [29]. In the first method, sCO_2 is used as a solvent for the coating material. For example, Quan et al. used sCO_2 to form alkyl ketene dimer coatings on paper surfaces [30]. Essentially, the material is dissolved in the supercritical phase and is then deposited on the surface. This was further explored by Olin et al. in an attempt to scale up through a semi-continuous spray process [31]. On the contrary, in the antisolvent method, a polymer is first dissolved in a solvent, and the mixture is then injected into the sCO_2 environment for coating. Since this is an extra step, the first method is typically preferred [32]. The issue with both these routes is the use of several chemical reagents, the non-uniformity of the coating, which is greatly influenced by the solubility of coating chemicals in sCO_2, and their restriction to surface applications (coating of porous materials is limited to those large pores which are impregnated in the relatively mild operative conditions and short times) [33]. Another use case of CO_2 for superhydrophobic surface fabrication is in the form of laser engravers. Pendurthi et al. used a CO_2 laser engraver to successfully fabricate nanostructured omniphobic and superomniphobic surfaces with a variety of materials [34]. Zhan et al. explored the use of CO_2 laser processing to fabricate a superhydrophobic polytetrafluoroethylene plate [35]. CO_2 lasers are inexpensive for superhydrophobic surface fabrication; however, they are currently not easy to scale up and cannot be applied to porous materials.

The fabrication protocol proposed here is straightforward, readily scalable with current production means, is free of hazardous chemicals, uses harmless compounds that can be easily recovered, and has added a positive environmental footprint as it provides a use-case for CO_2.

2. Methods

2.1. Materials

A 400x200x1mm copper sheet was purchased from Rapidonline. A series of flat copper pieces (20x30x1mm) were machined and polished using SiC paper (600, followed by 1200 and 2000). The samples were successively cleaned *via* sonication in acetone, ethanol and water before the $sCO_2 + H_2O$ exposure.

Cu powder with a maximum particle size of 75 μm was purchased from Sigma Aldrich (product number 207780). High purity 99.9% NaCl was used as a templating agent. 99.8%-pure CO_2 and water from the distiller were used (Aquatron automatic water stills A4000D, UK). All chemicals were purchased from Sigma Aldrich.

2.2. Fabrication of hierarchical porous copper

A hard templating method, similar to the one typically used in colloidal crystal, combined with sintering, was employed to prepare hierarchically porous Cu as follows. The Cu particles were mixed with NaCl crystals. Dry Cu and NaCl powders tend to be stratified under gravity force, resulting in inhomogeneous pores distribution. To overcome this issue, a mixture of Cu/NaCl particles was wetted with a minuscule amount of ethanol. Wetting facilitates the forming process. A saturated water/NaCl solution can be used instead of ethanol to avoid the crystal size change of NaCl. A cylindrical Cu mould was specifically made for shaping the particles' mixture in pellets. Before pouring wetted particles into the mould, its surface was covered by NaCl crystals to avoid sintering between Cu particles and the mould's walls. This was achieved by sequential immersion of the mould in a saturated water/NaCl solution and drying. The formed pellet was dried and then sintered by heating it up to 700 °C and maintained for 6 h under Ar/H atmosphere in the oven. After natural cooling, the pellet was then washed with distilled water until the template (NaCl) was entirely removed from the matrix (Fig. 1). It should be noted that after the synthesis, the NaCl can be recovered from the aqueous solution by evaporation, for example. Different salts, such as potassium chloride and lithium chloride, can also be used instead of NaCl. However, these have different water solubilities, which will affect how easily they can be washed out of the porous copper matrix. This coupled with the difference in grain geometry could influence the resulting pore size and structure, and hence the final contact angle.

2.3. Grafting protocol

Experiments were performed in a 25 ml SS316L Parr reactor model type W6886-01 from Parr Instrument Co, USA (Fig. 2). It is equipped with two in-line sapphire windows, a heating/cooling jacket and a magnetic stirrer, and operates from 10 to 100 °C up to 345 bar. The pressure is displayed by a pressure gauge (minimum scale 10 bar) and a digital display of the HPLC pump (minimum reading 1 PSI). The temperature is adjusted by circulating thermal oil using a Tecam circulator (C-40). Temperature is measured using a J-type thermocouple with an accuracy of 0.1 °C. The grafting protocol is described as follows:

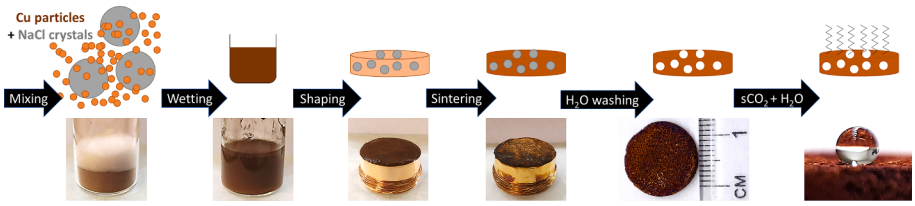

Fig. 1. Porous Cu preparation scheme.

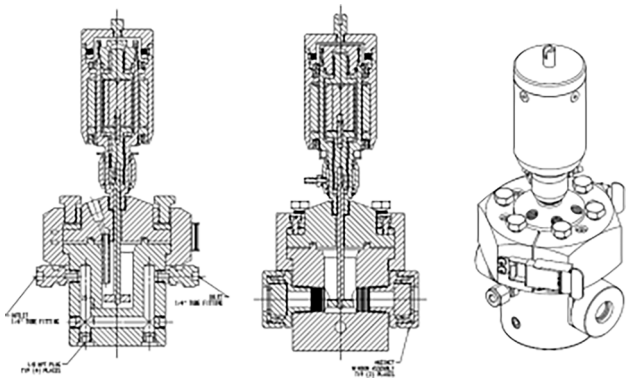

Fig. 2. The 25 ml SS316L Parr reactor model type W6886-01 (Parr Instrument Co, USA).

- The copper sample is ultrasonicated in ethanol (15 min) followed by water (15 min) and then dried using compressed air.
- ml of distilled water is placed in the reactor.
- The copper sample is placed in a plastic (polymer) sample holder.
- The holder is then placed in the reactor vessel.
- The reactor is then tightly screwed sealed.
- The Tecam circulator is used to raise the reactor temperature to 40 °C (313 K).
- The HPLC pump and inlet chiller are used to pump CO_2 to raise the reactor pressure to 20 MPa.
- The sample is maintained at this pressure (20 MPa) and temperature (40 °C) for 8 h.
- After 8 h, the CO_2 is slowly vented, and the Tecam circulator is turned off. Once ambient conditions are reached, the reactor is opened, and the sample is collected for further analysis.

Additional details regarding the protocol are described in a previous work [36].

2.4. Surface characterisation methods

Quanta 200 FEG Scanning Electron Microscopy (SEM) was used in high vacuum mode at 10 kV, 20 kV and 30 kV with a backscattered electron detector (BSED) and Everhart-Thornley Detector (ETD).

Bruker D8 Discover X-ray diffractometer was used with a LYNXEYE-XE detector using CuKα1 radiation (λ = 1.5418 Å) and Bragg-Brenato θ:2θ geometry. The data collection was carried out at room temperature, between 10° and 80°, with a step of 0.02° and a dwell time of 1.03 s per step. The EVA program was used to determine the phase composition of the material.

FTIR analysis of the Cu metal surfaces was performed by an FTIR spectrophotometer Vertex 80v (Bruker) operated in the reflectance mode using the accessory A513 (Bruker). During the measurements, the samples were kept at room temperature under vacuum conditions in the sample compartment evacuated down to the pressure of 2.3 mbar. The reflectance spectra were collected in the range of 450 cm− [1] to 3000 cm− [1] at the specular geometry with incident and reflected angles of 30^0, 45^0, and 60^0.

X-ray photoelectron spectroscopy (XPS) experiments were carried out on an ESCALAB 250Xi (Thermo Fisher Scientific) instrument with monochromated Al K_α (1486.6 eV) X-ray source and a hemispherical analyser operated at pass energies 40 eV and 150 eV for high resolution and survey spectra correspondently. The elemental depth profiling was performed by using a MAGCIS Ar ion gun (Thermo Fisher Scientific) operated in the monoatomic mode at Ar ion beam energy 1000 eV, corresponding to the sputtering rate of ~ 0.1 nm/sec. During the depth profiling process, XPS measurements were taken at regular intervals as the ion gun sputtered away the surface layers. The depth information is then obtained by correlating the acquired XPS spectra with the sputtering time and the known sputtering rate of the sample material. This method allows us to study the elemental composition and chemical states at various depths within the sample, providing valuable information on the surface modification and chemical distribution within the material.

The contact angle is experimentally determined at atmospheric pressure using the sessile drop method with the high-pressure equipment PD-E1700MD from Eurotechnica (Germany) [36] and using the DSA30 Drop Shape Analyzer from KRUSS (Germany). Each case is derived from the average of a total of 5 static contact angle values.

The dimensional measurements such as depth and periodicity of MS topographies, were assessed by employing a focus variation microscope (Alicona G5), which has a Vertical Resolution > 10 nm and Lateral Resolution > 400 nm.

2.5. MD simulations details

Molecular dynamics (MD) simulations were also employed to provide insights into the wetting mechanisms of grafted porous copper. A hierarchical roughness, such as the one investigated in this work, increases the formation probability of trapped air/vapour pockets on the surfaces. This further decreases the contact area between the droplet and the surface in the non-wetting regime. [37] Therefore, the wetting behaviour is not chemically homogenous, and the Cassie-Baxter equation to estimate the effective contact angle of the heterogeneous system is better suited. To this end, we attempted to obtain the droplet wetting fraction *f* by analysing the surface topography using the Alicona optical profilometer. A section of the 3D structure of the fabricated copper surface can be seen in Fig. 3.

The obtained image was post-processed using colour threshold options available on the ImageJ software. The goal was to band the various colour channels of the acquired image into two distinct channels. The first one represents the wetting fraction, which is depicted predominantly as orange, and the second is the non-wetting fraction, which is shown mainly in yellow-green. The two channels' pixel area ratio was then calculated to obtain the wetting fraction. Images from 3 different viewpoints were processed identically to improve statistics and resulted in an average wetting fraction of 0.417 ± 0.034.

A copper surface with a series of holes was reconstructed in VMD Topo Tools to match this wetting fraction [38]. Apart from the lateral, the vertical dimension of the roughness has been shown to play a role in the transition from Wetting to Cassie-Baxter state in textured surfaces [39–40]. To ensure this is captured in the model, the 2D profile of the 3D image was obtained (Fig. 4). The ratio between the height and diameter of the pore was calculated and found to be 3.12 ± 0.21. The depth of the

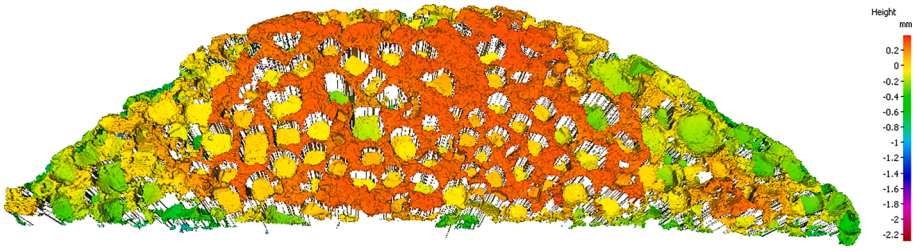

Fig. 3. 3D structural image of a section of the fabricated porous copper surface as obtained from the optical profilometer.

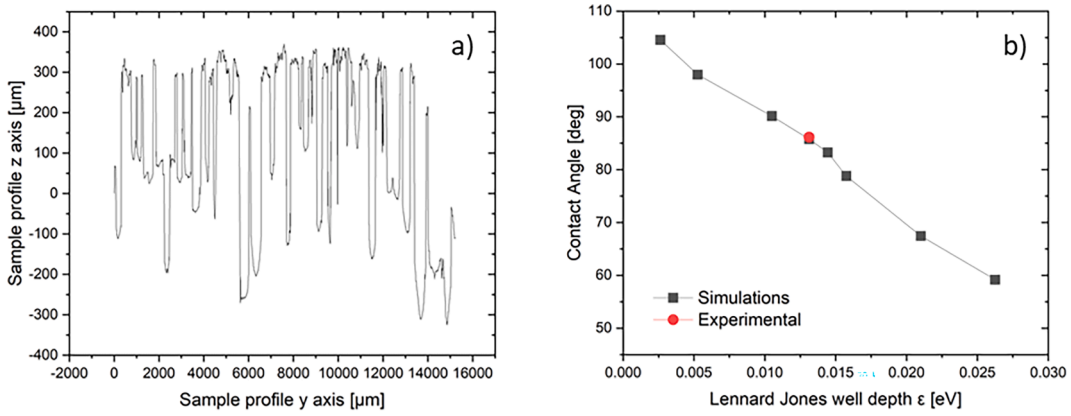

Fig. 4. 2D profile of the 3D image obtained from Alicona (a); Comparison of simulated contact angle of copper with experimental value for various well depth ε (b).

holes was then selected based on this ratio.

The Cassie-Baxter equation depends only on the roughness ratio, the solid/liquid contact area over the nominal area of the solid, i.e., it is independent of the absolute value of the pore size given a certain droplet size [41]. This said the geometrical characteristics of the pores used in this work have been successfully employed in the past to explain the different behaviour of silica of different topologies with respect to wetting by water [42]. Furthermore, a similar setup was previously used to explain different wetting characteristics of related MFI-, and TON-type zeolites [43]. Additionally, the roughness ratio was also previously successfully applied in models of molten $NaNO_3$ on carbon surfaces [44].

A bottom-to-top view of the porous surface can be seen in Fig. 5a and 5b. The white section inside the pores represents the non-wetted area, while the pink section the wetted area. A side view of the structure can be seen where the blue lines draw the wetted area, while the black to the non-wetted one.

A cylindrical droplet was deposited on an atomistically flat and roughened surface (Fig. 5a and 5d). This shape of the droplet was selected to limit droplet size effects, e.g., to eliminate the size-dependent contact line effects, reduce computational costs and increase simulation reliability [45]. The curvature-dependent surface tension is another size effect influencing the contact angle, which is accounted for *via* the modified Young's equation following a protocol established by Zhang

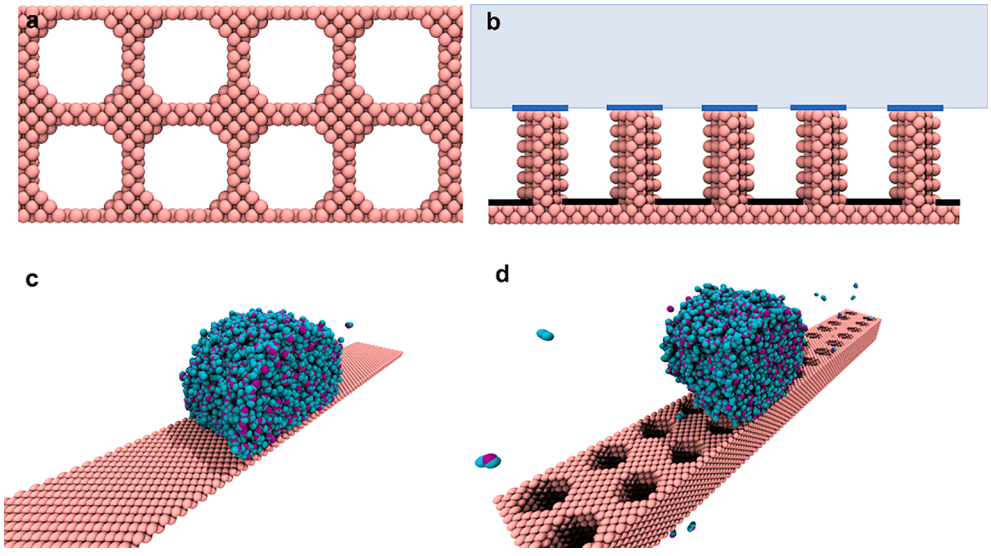

Fig. 5. a: Bottom-to-top view of the patterned surface; b: Side view of patterned surface; c: Water droplet on a flat copper surface; d: Water droplet on a patterned surface.

et al. for MD simulations in hydrophobic cases [46].

The simulation domain was periodic in all dimensions, with the dimensions $x = y = 2z$. Thermostating the slab atoms does not affect the resulting contact angle but significantly reduces the required computational time [47]; hence the slab of atoms remained frozen throughout the simulation. The liquid is thermalised in the constant number of particles, constant volume and constant temperature (NVT) ensemble for 40 ns. This is followed by 20 ns of data collection. To prevent metastability issues, the temperature of the liquid is slightly increased in the hydrophilic (Wenzel) simulations [48]. All simulations are performed with a timestep of 0.002 ps. The Particle-Particle Particle-Mesh (PPPM) solver was used to calculate the long-range electrostatic interactions with an accuracy of 10^{-5}. [49] Water was simulated using the SPC/E potential. This water model has been extensively used in interface simulations; in particular, SPC/E water has been used to investigate the wetting of hydrophobic porous cavities [43]. For copper, the parameters provided by Lv et al. have been shown to accurately predict the density and surface energy of the copper surface [50]. Copper/water cross terms following the Lorentz-Berthelot rules were unable to reproduce the contact angle of the flat metal surface, even after applying adequate size effect corrections. The depth of the potential well ε in the cross-term Lennard-Jones parameters between the water and the copper was thus tuned (Fig. 4b) to match the experimental macroscopic value measured on a smooth flat copper surface, $\theta = 86°$.

3. Results

After subjecting flat Cu samples to $sCO_2 + H_2O$ treatment, their water contact angle changed from 86 ± 2° to 97 ± 3° - Fig. 6a and 6b. Therefore, a desirable wetting-to-nonwetting transition was achieved (transition from CA < 90° to CA > 90°). Classical capillary theory dictates that CA < 90° results in the spontaneous adsorption of liquid into a pore, while CA > 90° implies that the pore stays dry unless the liquid is intruded inside by an external force.

This effect was evident for porous copper samples. Before $sCO_2 + H_2O$ treatment, porous copper adsorbs water – Fig. 6c and Video S1. On the contrary, after the $sCO_2 + H_2O$ treatment, water bounces off the porous copper surface and reveals the observable contact angle of 146 ± 5° – Fig. 6d and Video S2.

A similar effect was evident from MD simulation campaign. First, the water-copper interactions were tuned to match the contact angle value of 86°, which was measured on the untreated Cu – Fig. 4b and 4e. This was then used to simulate the wetting behaviour on the patterned surface. Adsorption of water into the pores was evident (Wenzel state) – Fig. 6g. Next, the water-copper interactions were tuned to match the contact angle value of 97°, which was measured on the $sCO_2 + H_2O$ treated Cu – Fig. 6f. This was then used to simulate the wetting behaviour on the patterned surface. The water was not adsorbed into the pores (Cassie-Baxter state), demonstrating the contact angle of 133° – Fig. 6h.

Copper samples before and after $sCO_2 + H_2O$ treatment were characterised *via* XRD, FTIR and XPS depth profiling. XRD analysis reveals that $sCO_2 + H_2O$ treatment does not bring new crystalline phases to the sample, as peak positions are consistent with metallic copper (Fig. 7) [51] and a minor quantity of Cu_2O for both cases. However, after the treatment, one can notice a slight increase in the copper oxide phase (Fig. 7). Simulated patterns for Cu and Cu_2O were taken from Crystallography Open Database: ID 7101264 and ID 1000063, respectively.

FTIR analysis confirms considerable enhancement of highly hydrophobic asymmetric and symmetric CH_2 and CH_3 groups after $sCO_2 + H_2O$ treatment (Fig. 8).

XPS-depth profiling characterisation is in line with FTIR analysis (Fig. 9). The Cu2p and O1s spectra evidence a surface layer of Cu_2O with a thickness below 10 nm. Pure copper is known to readily oxidise in ambient conditions and form Cu_2O and CuO phases. In fact, XPS spectra for both treated and untreated samples exhibit spectral lines in the energy range between 932 and 933 eV, characteristic of the CuO_x species. [52] The C1s spectra show maximum centred at 285 eV characteristic of C–C and C–H bonds [53]. Virtually no signatures of C-O, and C = O groups were observed in the C1s and O1s spectra. The atomic concentrations of carbon and oxygen gradually decrease deeper into the material. The initial carbon concentration on the treated surface is higher than that on the untreated surface (Fig. 9h vs 9 g). Notably, the carbon-containing surface layer in the treated sample was found to be ~ 10 times thicker than that in the untreated sample, with a thickness of 5 nm and ~ 40 nm, respectively (Fig. 9h vs 9 g). The latter observation is in accord with the reflectance FTIR results (Fig. 8).

Porous copper samples were characterised by SEM. Templating followed by annealing results in a highly textured Cu with hierarchical macro-nanoporosity (Fig. 10). Large (hundreds of microns) pores are the result of NaCl templating. They are interconnected with a secondary network of pores with a considerably smaller length scale range (microns) – the result of interparticle porosity. Finally, nanoroughness is

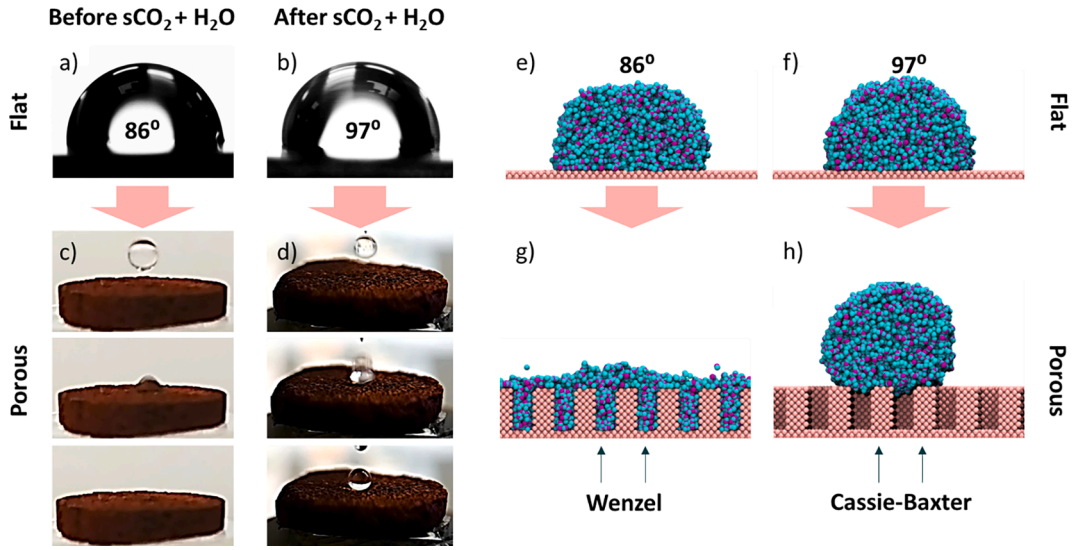

Fig. 6. Water contact angle on a flat Cu before (a) and after (b) $sCO_2 + H_2O$ treatment. Snapshots of a water drop falling onto the porous copper before (c) and after (d) $sCO_2 + H_2O$ treatment. For more details, see Videos S1 and S2. Water contact angle on a flat Cu obtained from MD simulations (e and f) and corresponding interaction with porous Cu (g and h).

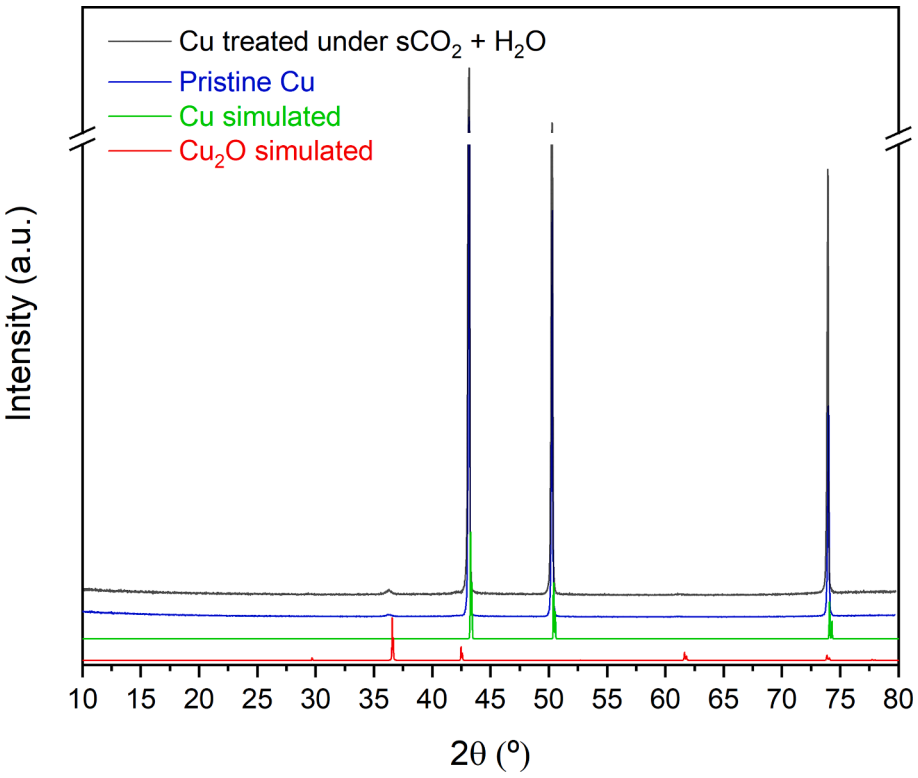

Fig. 7. XRD analysis of the Cu sample before and after $sCO_2 + H_2O$ treatment.

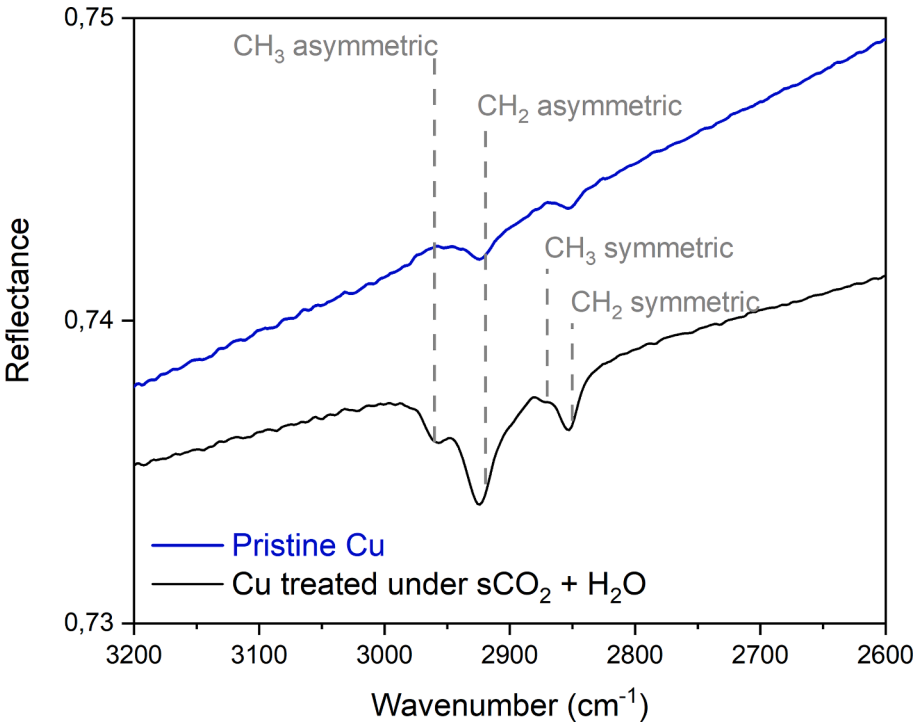

Fig. 8. FTIR spectra from the copper samples before and after $sCO_2 + H_2O$ treatment. The spectra were acquired in the reflectance mode with the incident and reflected angles of 45^0 with respect to the surface normal. The spectra were referenced to a glass mirror surface.

observed at higher magnification. Macro- and nanoscale hierarchically porous structures have been shown to considerably increase surface roughness, which is an essential prerequisite for superhydrophobicity.

It should be noted that $sCO_2 + H_2O$ treatment had an effect on the topology of Cu at the nanoscale, presumably removing copper oxide flakes and enabling homogeneous nanoscale roughness (Fig. 10 and Figure S1).

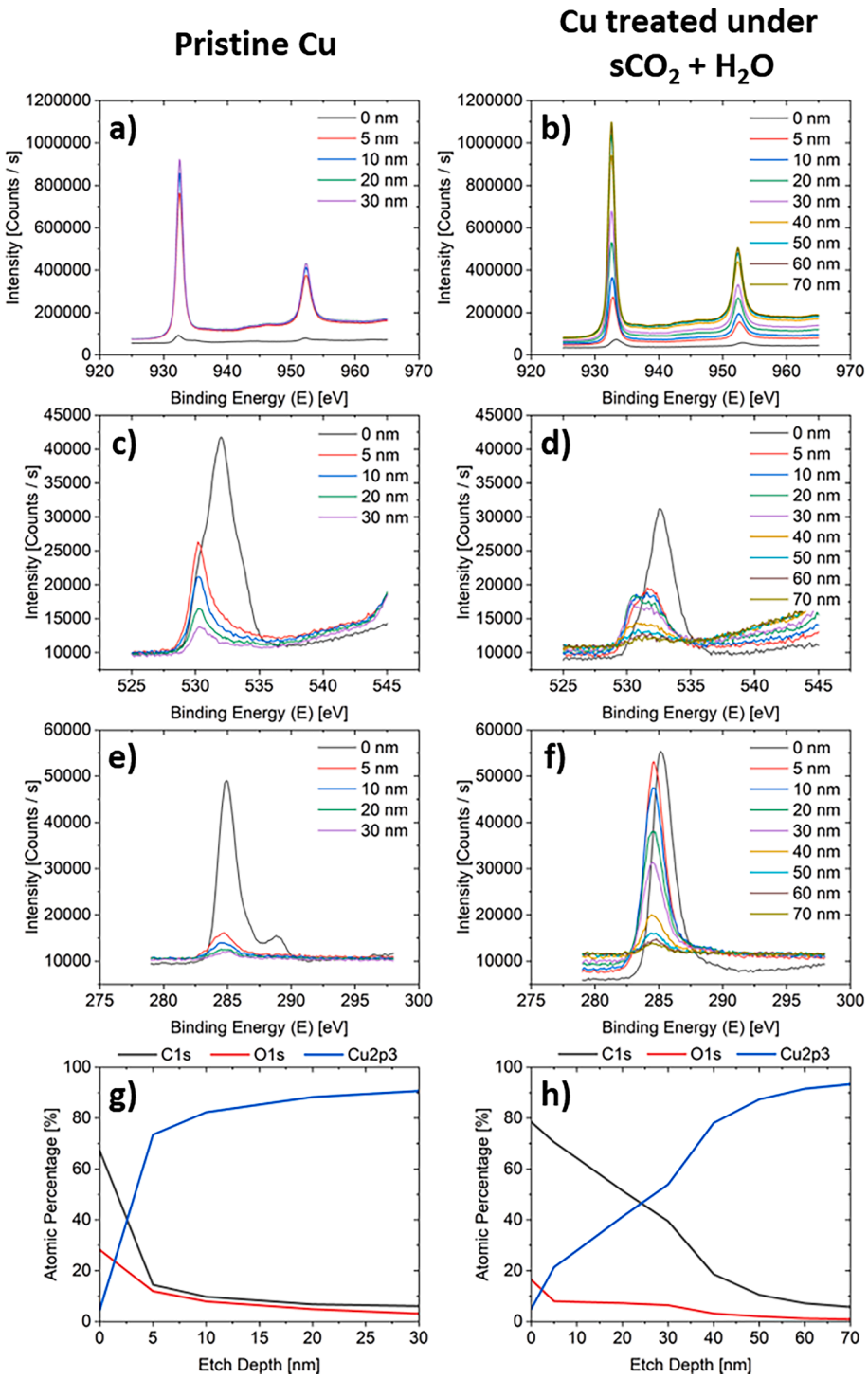

Fig. 9. XPS scans for the untreated (left column) and treated (right column) copper surface: Cu2ps (a and b), O1s (c and d), C1s (e and f) and depth profiling (g and h).

4. Discussion

In this section, we discuss two aspects of the obtained results: the effect of roughness and the effect of sCO_2 + H_2O treatment on the wettability of copper.

Effect of roughness. Before sCO_2 + H_2O treatment, porous Cu samples absorbed the water droplet completely (Fig. 6c and Video S1). This behaviour is expected as a smooth copper surface is hydrophilic, with a CA of c.a. 86°, as measured in this work (Fig. 6a) and reported in the literature. [54] This is consistent with Wenzel's theory, which predicts that roughness amplifies the wetting behaviour [55]. Hydrophilic surfaces become more hydrophilic after being roughened, and the state in which the liquid spontaneously wets the roughnesses is energetically favoured. This has been investigated for a wide range of area magnification factors (roughness) by Shibuichi et al. [56] The authors modified the roughness parameter of the Wenzel equation with two variables describing the fractal dimensions of the roughened surfaces and verified it experimentally.

As can be seen from Fig. 6d and 10, porous copper treated with sCO_2 + H_2O no longer absorbs water. In particular, water droplet bouncing

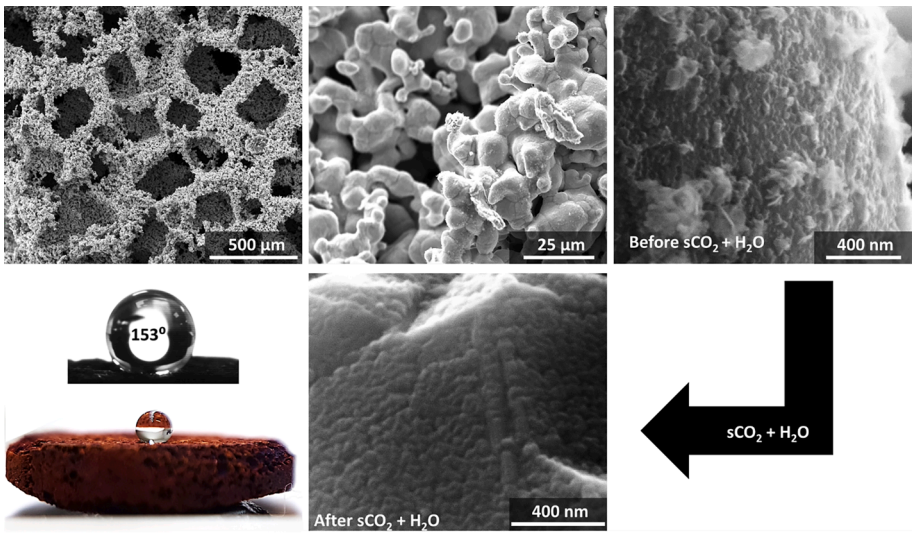

Fig. 10. Top row: SEM images of the porous copper sample before $sCO_2 + H_2O$ treatment; Bottom row: Left: Water contact angle and SEM image of the copper sample after $sCO_2 + H_2O$ treatment; Right: SEM image of sample surface after $sCO_2 + H_2O$ treatment.

(Video S2) and CA of 146 ± 5° (Fig. 6d and 10) were achieved. Such considerable enhancement of non-wetting behaviour compared to smooth copper treated with $sCO_2 + H_2O$ (CA of c.a. 97°) can be explained by Cassie-Baxter theory. The latter predicts that surface roughness enhances the contact angle in the hydrophobic regime. [57–58].

Crick and Parkin investigated a broad range of surfaces and established a relationship between water contact angle and the number of bounces [59]. They defined one bounce as a sufficient condition for superhydrophobicity, which is only observed in cases where the contact angle is>151°. They also investigated the effect of topography on water pinning. Certain arrangements can promote water pinning, which increases the surface-water adhesive force and reduces the rebound momentum of the water droplet. In fact, surfaces that promoted water pinning had to typically exhibit a contact angle higher than 156° to achieve more than one bounce. Their observations are in excellent agreement with the behaviour observed in this work. CA was measured to be 146 ± 5° after $sCO_2 + H_2O$ treatment, and a single bounce was observed, followed by pinning (Fig. 6d and Video S2). These conditions are satisfactory to define the porous copper treated with $sCO_2 + H_2O$ as a superhydrophobic material.

To better understand the effect of roughness, the contact angle of water on a patterned surface was simulated using the cross-term parameters corresponding to water CA of 86° (Fig. 6e) and 97° on a flat Cu (Fig. 6f). The results revealed that for the case of 86°, the water was adsorbed into the roughness (Fig. 6g), while for the case of 97°, the roughness was maintained dry, and a water contact angle of 133° was achieved (Fig. 6h). The value of 133° is in reasonable agreement with the value of 129° obtained directly from the Cassie Baxter formula for a flat surface-contact angle of 97° and a wetting fraction of 0.417. It demonstrates the validity of the Cassie-Baxter equation at the nanoscale. The applicability of the Cassie-Baxter equation for uniformly rough surfaces is, of course, well established [60]. As Gao and McGarthy suggested, the Cassie-Baxter theory depends on the local angle at the triple contact line, which in this case is global as the surface is uniformly textured [61].

Interestingly, it can be used to validate the physical contribution to superhydrophobicity, even though the latter is a multiscale phenomenon. A broader study involving many patterned surfaces is necessary to solidify this. Nevertheless, the predicted contact angle is lower than the one measured experimentally (146°), which may be due to hierarchical roughness in the experiment and a non-hierarchical one in the simulations.

From the discussion above, the effect of roughness on the effective wettability of porous copper can be reasoned within the classical theories. On the other hand, an intriguing question remains regarding the observed wetting-to-nonwetting transition achieved *via* $sCO_2 + H_2O$ treatment (Fig. 6a – 6d). To this end, surface characterisation techniques were employed to investigate the effect of the processing steps on surface chemistry. These results are discussed below.

Effect of grafting *via* $sCO_2 + H_2O$ treatment: Hypothesis 1 – the effect of atmospherically adsorbed CH_x groups. Characterisation and interpretation of surfaces containing CH_x groups are challenging from a methodological point of view. These groups are present in the atmosphere and can be detected in nearly every sample which was exposed to the environment. This is the case of pristine copper (Fig. 8). In fact, the adsorption of CH_x groups from the environment is so pronounced that it emerges as a promising route for the atmosphere-mediated production of superhydrophobic surfaces [2]. Therefore, we cannot exclude that the observed non-wetting behaviour reported in this work is due to the adsorption of atmospheric CH_x groups. Nevertheless, we hypothesise that this mechanism is not predominant due to several observations listed below.

First, the water CA evolution due to atmospheric adsorption of CH_x groups is typically on the order of days, if not weeks [2,62–63]. On the contrary, our experiments recorded the effect on the CA immediately after $sCO_2 + H_2O$ treatment.

Second, after $sCO_2 + H_2O$ treatment, the quantity of CH_x groups is considerably higher compared to the pristine Cu (Fig. 8). In particular, XPS depth profiling reveals the thickness of the carbon-containing layer to be approximately one order of magnitude higher for the treated copper (Fig. 9g vs 9 h).

Effect of grafting *via* $sCO_2 + H_2O$ treatment: Hypothesis 2 – CO_2 hydrogenation as a source of CH_x groups. Activation of CO_2 *via* chemisorbed negatively charged species is a favourable reaction pathway. It has been previously reported on polycrystalline Cu surfaces coupled with weakly physisorbed CO_2 species [64]. Deng et al. investigated the chemical nature of Cu in the presence of low concentrations of H_2O and CO_2 in a high vacuum chamber. They confirmed the presence of negatively charged carbonate species on the surface and the presence of formate, methoxy and residuals in the form of graphite or CH_x hydrocarbon fragments [65]. H_2O might provide the hydrogen required to facilitate these reactions. Such reactions have been shown to occur *via* hydrogenation of the adsorbed CO2 [66]. More specifically, a well-

known Fischer–Tropsch reaction can be used to synthesise valuable hydrocarbons [67]:

$$nCO_2 + 3nH_2 \rightarrow (-CH_2-)_n + 2nH_2O \rightarrow Hydrocarbons \quad (1)$$

It is known that CO_2 pressure improves synthesis efficiency [67–68] and that Cu is a good catalyst [69]. The intermediate steps for the transformation of CO_2 to hydrocarbons are either through formate or a carboxyl pathway [70]. The former has been found to be more abundant on catalyst surfaces [71]. In the proposed formate reaction route, CO_2 reacts with surface atomic H forming HCOO via either an Eley–Rideal (ER) or Langmuir–Hinshelwood (LH) mechanism [72]. These reactions are explained in detail in the literature [70,72]. However, CO_2 hydrogenation is not a straightforward mechanism, and it is influenced by various mechanisms [73–74].

Nevertheless, CO_2 hydrogenation was reported to transform CO_2 and water into valuable hydrocarbons *via* photo- [75] or electrochemical [67] routes. It was reported that CH_2 and CH_3 groups are intermediate products of these reactions [75]. In these references, [67,75] obviously, an external source of electrons was available to enable CO_2 hydrogenation. In the current work, the source of electrons may be the oxidation of copper, which is evident from XRD and XPS characterisation (oxide layer thickness is around one order of magnitude large after $sCO_2 + H_2O$ treatment – Fig. 9g vs 9 h). Here, Cu is at the same time a reaction site binding CH_x and the reactant donating electrons via the formation of surface oxides, CuO_x.

It is known that Cu does not directly react with water. However, the presence of oxygen and CO_2 may provoke certain reactions. Carbonic acid (H_2CO_3) formed due to the presence of CO_2 in the water dissociates into HCO_3^- and hydrogen ions (H^+). A surface copper oxide (Fig. 7) then reacts with H^+ to form water. As a result, the copper at the surface that is now in its ionic form dissolves. Finally, the copper surface, now unprotected by the oxide, is again exposed to water and H^+ allowing the process to recur [76].

At this point, based on our observations and reported literature, we only have grounds to speculate that $sCO_2 + H_2O$ treatment of copper has all the ingredients for a CO_2 hydrogenation reaction to transform CO_2 and H_2O into CH_x:

- Source of C and H;
- High pressure to trigger CO_2 hydrogenation;
- Copper oxidation as a source of electrons;
- Copper as a catalyst, and as a result, the preferential binding site for CH_x groups.

The viability of this hypothesis will be verified in a future combined experimental/theoretical work, where selected Cu surfaces will be subjected to different experimental conditions and rare event density functional theory calculations will be performed to identify the possible reaction path, energetics and kinetics of these processes. If Hypothesis 2 is correct, then this method can be applied to many more metals and their combinations. The efficiency will depend on the catalytic activity of each metal.

5. A potential application and durability assessment

5.1. Oil-water separation

The proposed method has a potential to be scaled up using existing production means since large supercritical CO_2 vessels, hydraulic presses and furnaces are already available in the industry. After economic viability and environmental impact evaluation, this may allow large-scale manufacturing of superhydrophobic surfaces and porous materials.

The fabricated superhydrophobic porous copper is evaluated for oil–water separation applications. A synthetic polyol ester lubricant Emkarate® RL 68H, typically used in refrigeration and air-conditioning compressors, is first coloured by Oil Red dye (Sigma Aldrich CAS 1320–06-5) and then mixed with water.

Four stages of oil separation are shown in Fig. 11:

1. The oil droplet is attached to the bottom of the vial using a syringe and a needle.
2. A piece of superhydrophobic porous copper is brought into contact with the oil droplet.
3. The oil penetrates superhydrophobic porous copper.
4. The air located in the pores is displaced.

The performed oil separation can also be seen in the videos available in supplementary materials.

Separation efficiency is commonly calculated as the ratio of the mass of extracted oil to the initial mass. In our case, to determine the masses of oil droplets submerged in water that were required for the calculation, we processed images captured before and after separation. First, the water–oil boundaries were defined, and later, a 3D reconstruction of the drops was obtained (Figure S2). Knowing the volume of the droplets and the density of Emkarate® RL 68H oil (0.977 g/cm3), the masses were determined to be 12.97 mg before and 0.0553 mg after separation. The resulting efficiency was 95.7 ± 2%. The separation efficiency value obtained in our study is consistent with those reported by other researchers [77–79].

It is worth noting that the residual oil droplets observed at the bottom could be attributed to the cohesion between the oil and the glass, rather than an inherent limitation of the porous copper material. Future work will involve more rigorous testing and quantification of the separation efficiency, providing a clearer understanding of the material's performance in practical applications.

5.2. Durability assessment

The durability of the hydrophobic grafting is also evaluated through abrasion and water-impact tests following known and established protocols [80]. For abrasion, the surface is attached to a stainless-steel slab and is then moved back and forth at a distance of 12 cm on a SiC sandpaper under a total load of 289 g (including the sample). For the water impact test, the sample is maintained stable using a utility clamp and positioned vertically under an aggressive constant water flow with a velocity of 2.8 m/s and a weaker flow of 0.2 m/s. The high flow rate is meant to emulate flow-like conditions in pipes, while the lower water flow is essentially similar to dripping water droplets on the surface.

The durability of the surface with respect to abrasion is evaluated via contact angle measurements after every 5 passes (Fig. 12 Right). In all assessments, contact angle measurements are averaged over 3 different spots on the surface. For the first ten passes the contact angle is stable. Following this, a gradual decline is observed. After twenty-five passes the contact angle is close to the base. This degree of durability is reasonable and in agreement with other quoted "durable" superhydrophobic surfaces that demonstrate similar degrees of decay during abrasion [81].

In terms of durability under flow, the effect of the water velocity is apparent. The contact angle rapidly decreases at larger velocities approaching values close to that of unprocessed copper in a short time frame (Fig. 12 Left). Lower velocities have less impact on the hydrophobic grafting. The surface is found to be stable even after 20 min of continuous exposure to water flow.

Lastly, it should be noted that the contact angle of water on the grafted copper surface is found to be stable after 6 months. This indicates that the grafting has good long-term stability. The fact that no contact angle increase is observed suggests that either the majority of absorption transpires in early stages and no more vacant sites are available (Hypothesis 1), or most likely the grafting is attained through a catalytic pathway (Hypothesis 2).

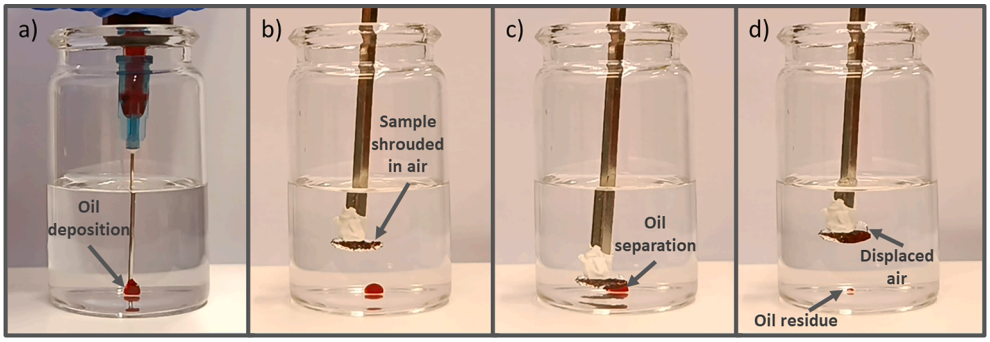

Fig. 11. Demonstration of oil separation from water: a) deposition of the oil drop on the bottom of the vial; b) superhydrophobic porous copper approaching oil droplet; c) oil absorption by the superhydrophobic porous copper; d) after oil separation images of the porous copper sample.

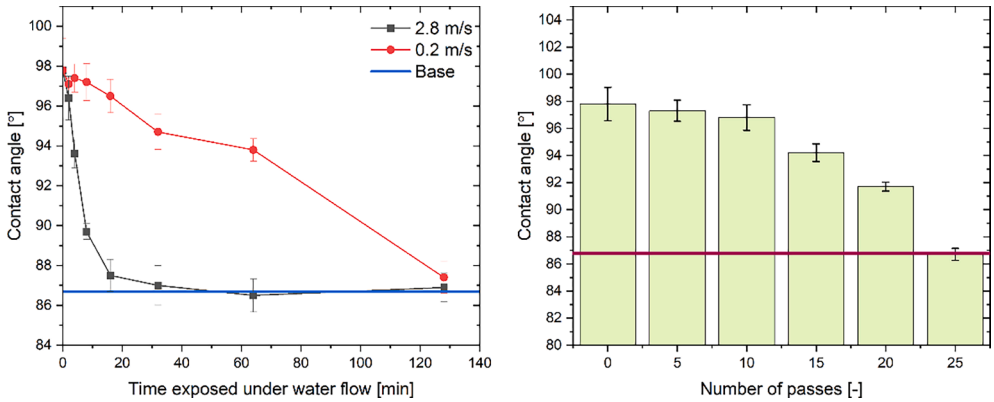

Fig. 12. Left: Effect of water impact on grafting durability; Right: Effect of abrasion on grafting durability (red line resents the contact angle value of copper prior to CO_2 + water treatment). (For interpretation of the references to colour in this figure legend, the reader is referred to the web version of this article.)

6. Conclusions

This work proposes a facile scalable process to fabricate superhydrophobic metallic surfaces and porous materials, which provides a use case for stored CO_2. Unexpectedly, we discovered that $sCO_2 + H_2O$ treatment of copper increases its hydrophobicity and results in a wetting-to-nonwetting transition for water. This effect is due to copper surface finishing by highly hydrophobic CH_2 and CH_3 groups. We hypothesise that CO_2 hydrogenation reactions are responsible for such a grafting. The hydrophobicity of copper was further reinforced by hierarchical roughness generated through a simple templating and annealing protocol of copper particles. Hence, a combination of $sCO_2 + H_2O$ treatment and hierarchical topology resulted in superhydrophobic copper surfaces. The synergetic effect of roughness and chemical grafting is indirectly verified through MD simulations that validate the Cassie-Baxter theorem at the nanoscale and confirm that topological contributions alone are insufficient to obtain a superhydrophobic surface. The fabricated superhydrophobic porous material is shown to perform well in an oil–water separation test. Furthermore, the grafted groups are found to have good durability in terms of abrasion, water impact and long-term stability. Conclusively, this simple, scalable protocol may enable a new sustainable pathway for the mass production of durable superhydrophobic surfaces and porous metals for various established and emerging applications.

CRediT authorship contribution statement

Argyrios Anagnostopoulos: Formal analysis, Investigation, Visualization, Methodology, Writing – original draft. **Artem Nikulin:** Formal analysis, Investigation, Visualization. **Sandra Knauer:** Formal analysis, Investigation. **Oleksandr Bondarchuk:** Formal analysis, Investigation, Visualization. **Maria Elena Navarro Rivero:** Formal analysis, Investigation. **Tiejun Lu:** Formal analysis, Investigation. **Themistoklis Karkantonis:** Formal analysis, Investigation. **Elena Palomo del Barrio:** Investigation, Supervision. **Mirosław A. Chorążewski:** Investigation, Supervision. **Yongliang Li:** Investigation, Supervision, Writing – review & editing. **Yulong Ding:** Investigation, Supervision, Writing – review & editing. **Simone Meloni:** Conceptualization, Methodology, Supervision, Writing – review & editing. **Yaroslav Grosu:** Conceptualization, Methodology, Supervision, Writing – review & editing.

Declaration of Competing Interest

The authors declare that they have no known competing financial interests or personal relationships that could have appeared to influence the work reported in this paper.

Data availability

Data will be made available on request.

Acknowledgements

This project leading to this application has received funding from the European Union's Horizon 2020 research and innovation programme under grant agreement No 101017858. The work has been performed with the financial support of the National Science Centre (Poland) under Decision No. 2018/31/B/ST8/00599.

Appendix A. Supplementary data

Supplementary data to this article can be found online at https://doi.

org/10.1016/j.apsusc.2023.157546.

References

[1] S. Parvate, P. Dixit, S. Chattopadhyay, Superhydrophobic Surfaces: Insights from Theory and Experiment, J. Phys. Chem 2020 (2020), https://doi.org/10.1021/acs.jpcb.9b08567.

[2] X. Yan, Z. Huang, S. Sett, J. Oh, H. Cha, L. Li, L. Feng, Y. Wu, C. Zhao, D. Orejon, F. Chen, N. Miljkovic, Atmosphere-Mediated Superhydrophobicity of Rationally Designed Micro/Nanostructured Surfaces, ACS Nano 13 (4) (2019) 4160–4173, https://doi.org/10.1021/ACSNANO.8B09106/SUPPL_FILE/NN8B09106_SI_005.AVI.

[3] Y. Liu, X. Cao, J. Shi, B. Shen, J. Huang, J. Hu, Z. Chen, Y. Lai, A Superhydrophobic TPU/CNTs@SiO2 Coating with Excellent Mechanical Durability and Chemical Stability for Sustainable Anti-Fouling and Anti-Corrosion, Chem. Eng. J. 434 (2022), 134605, https://doi.org/10.1016/J.CEJ.2022.134605.

[4] Y. Liu, H. Gu, Y. Jia, J. Liu, H. Zhang, R. Wang, B. Zhang, H. Zhang, Q. Zhang, Design and Preparation of Biomimetic Polydimethylsiloxane (PDMS) Films with Superhydrophobic, Self-Healing and Drag Reduction Properties via Replication of Shark Skin and SI-ATRP, Chem. Eng. J. 356 (2019) 318–328, https://doi.org/10.1016/J.CEJ.2018.09.022.

[5] J. Li, W. Jiao, Y. Wang, Y. Yin, X. He, Spraying Pressure-Tuning for the Fabrication of the Tunable Adhesion Superhydrophobic Coatings between Lotus Effect and Petal Effect and Their Anti-Icing Performance, Chem. Eng. J. 434 (2022), 134710, https://doi.org/10.1016/J.CEJ.2022.134710.

[6] W. Ma, Z. Jiang, T. Lu, R. Xiong, C. Huang, Lightweight, Elastic and Superhydrophobic Multifunctional Nanofibrous Aerogel for Self-Cleaning, Oil/Water Separation and Pressure Sensing, Chem. Eng. J. 430 (2022), 132989, https://doi.org/10.1016/J.CEJ.2021.132989.

[7] A.K. Sasmal, C. Mondal, A.K. Sinha, S.S. Gauri, J. Pal, T. Aditya, M. Ganguly, S. Dey, T. Pal, Fabrication of Superhydrophobic Copper Surface on Various Substrates for Roll-off, Self-Cleaning, and Water/Oil Separation, ACS Appl. Mater. Interfaces 6 (24) (2014) 22034–22043, https://doi.org/10.1021/AM5072892/SUPPL_FILE/AM5072892_SI_004.AVI.

[8] L. Kang, Q. Zeng, B. Wang, J. Zeng, B. Liao, H. Wu, Z. Cheng, X. Guo, Facile Fabrication of Multi Superlyophobic Nano Soil Coated-Mesh Surface with Excellent Corrosion Resistance for Efficient Immiscible Liquids Separation, Sep. Purif. Technol. (2022,) 284, https://doi.org/10.1016/j.seppur.2021.120266.

[9] L. Kang, L. Shi, Q. Zeng, B. Liao, B. Wang, X. Guo, Melamine Resin-Coated Lignocellulose Fibers with Robust Superhydrophobicity for Highly Effective Oil/Water Separation, Sep. Purif. Technol. (2021) 279, https://doi.org/10.1016/j.seppur.2021.119737.

[10] X. Chen, P. Wang, D. Zhang, J. Ou, Rational Fabrication of Superhydrophobic Surfaces with Coalescence-Induced Droplet Jumping Behavior for Atmospheric Corrosion Protection, Chem. Eng. J. 428 (2022), 132029, https://doi.org/10.1016/J.CEJ.2021.132029.

[11] Z. Wang, S. Peng, L. Wu, Z. Weng, Construction of Ultra-Long Service Life Self-Cleaning Slippery Surface on Superhydrophobicity Functionalized by ATRP Treatment, Chem. Eng. J. 428 (2022), 130997, https://doi.org/10.1016/J.CEJ.2021.130997.

[12] F. Sahin, N. Celik, A. Ceylan, S. Pekdemir, M. Ruzi, M.S. Onses, Antifouling Superhydrophobic Surfaces with Bactericidal and SERS Activity, Chem. Eng. J. 431 (2022), 133445, https://doi.org/10.1016/J.CEJ.2021.133445.

[13] Y. Zhan, S. Yu, A. Amirfazli, A. Rahim Siddiqui, W. Li, Recent Advances in Antibacterial Superhydrophobic Coatings, Adv. Eng. Mater. (2022), https://doi.org/10.1002/adem.202101053.

[14] Y. Zhan, S. Yu, A. Amirfazli, A.R. Siddiqui, W. Li, Magnetically Responsive Superhydrophobic Surfaces for Microdroplet Manipulation, Adv. Mater. Interfaces 9 (5) (2022), https://doi.org/10.1002/admi.202102010.

[15] W. Li, Y. Zhan, A. Amirfazli, A.R. Siddiqui, S. Yu, Recent Progress in Stimulus-Responsive Superhydrophobic Surfaces, Prog. Org. Coatings 168 (2022), 106877, https://doi.org/10.1016/J.PORGCOAT.2022.106877.

[16] Y. Zhan, W. Li, A. Amirfazli, S. Yu, Recent Advances in Shape Memory Superhydrophobic Surfaces: Concepts, Mechanism, Classification, Applications and Challenges, Polymer (Guildf). 256 (2022), 125193, https://doi.org/10.1016/J.POLYMER.2022.125193.

[17] Superhydrophobic Coatings Market | 2022 - 27 | Industry Share, Size, Growth - Mordor Intelligence https://www.mordorintelligence.com/industry-reports/superhydrophobic-coatings-market.

[18] S.T. Yohe, J.D. Freedman, E.J. Falde, Y.L. Colson, M.W. Grinstaff, A Mechanistic Study of Wetting Superhydrophobic Porous 3D Meshes, Adv. Funct. Mater. 23 (29) (2013) 3628–3637, https://doi.org/10.1002/ADFM.201203111.

[19] G. McHale, N.J. Shirtcliffe, M.I. Newton, Super-Hydrophobic and Super-Wetting Surfaces: Analytical Potential? Analyst 129 (4) (2004) 284–287, https://doi.org/10.1039/B400567H.

[20] M.T.Z. Myint, G.L. Hornyak, J. Dutta, One Pot Synthesis of Opposing 'Rose Petal' and 'Lotus Leaf' Superhydrophobic Materials with Zinc Oxide Nanorods, J. Colloid Interface Sci. 415 (2014) 32–38, https://doi.org/10.1016/J.JCIS.2013.10.015.

[21] C. Lu, Y. Gao, S. Yu, H. Zhou, X. Wang, L. Li, Non-Fluorinated Flexible Superhydrophobic Surface with Excellent Mechanical Durability and Self-Cleaning Performance, ACS Appl. Mater. Interfaces 14 (3) (2022) 4750–4758, https://doi.org/10.1021/ACSAMI.1C21840/SUPPL_FILE/AM1C21840_SI_005.MP4.

[22] K. Ellinas, P. Dimitrakellis, P. Sarkiris, E. Gogolides, A Review of Fabrication Methods, Properties and Applications of Superhydrophobic Metals. (2021).

[23] M. Cui, H. Huang, C. Wang, L. Zhang, J. Yan, Achieving Superhydrophobicity of Zr-Based Metallic Glass Surfaces with Tunable Adhesion by Nanosecond Laser Ablation and Annealing, ACS Appl. Mater. Interfaces 14 (34) (2022) 39567–39576, https://doi.org/10.1021/ACSAMI.2C10546/ASSET/IMAGES/LARGE/AM2C10546_0007.JPEG.

[24] C.H. Moon, S. Yasmeen, K. Park, H. Gaiji, C. Chung, H. Kim, H.S. Moon, J.W. Choi, H.B.R. Lee, Icephobic Coating through a Self-Formed Superhydrophobic Surface Using a Polymer and Microsized Particles, ACS Appl. Mater. Interfaces 14 (2) (2022) 3334–3343, https://doi.org/10.1021/ACSAMI.1C22404/SUPPL_FILE/AM1C22404_SI_002.MP4.

[25] J. Li, Y. Zhou, W. Wang, C. Xu, L. Ren, Superhydrophobic Copper Surface Textured by Laser for Delayed Icing Phenomenon. (2020), https://doi.org/10.1021/acs.langmuir.9b02273.

[26] R. Yamamoto, D. Kowalski, R. Zhu, K. Wada, Y. Sato, S. Kitano, C. Zhu, Y. Aoki, H. Habazaki, Fabrication of Superhydrophobic Copper Metal Nanowire Surfaces with High Thermal Conductivity, Appl. Surf. Sci. 537 (2021), 147854, https://doi.org/10.1016/J.APSUSC.2020.147854.

[27] S.M.A. Mousavi, R. Pitchumani, A Study of Corrosion on Electrodeposited Superhydrophobic Copper Surfaces, Corros. Sci. 186 (2021), 109420, https://doi.org/10.1016/J.CORSCI.2021.109420.

[28] X. Yin, Z. Wang, Y. Shen, P. Mu, G. Zhu, J. Li, Facile Fabrication of Superhydrophobic Copper Hydroxide Coated Mesh for Effective Separation of Water-in-Oil Emulsions, Sep. Purif. Technol. 230 (2020), 115856, https://doi.org/10.1016/J.SEPPUR.2019.115856.

[29] X. Zhang, S. Heinonen, E. Levänen, Applications of Supercritical Carbon Dioxide in Materials Processing and Synthesis, RSC Adv. 4 (105) (2014) 61137–61152, https://doi.org/10.1039/C4RA10662H.

[30] C. Quan, O. Werner, L. Wågberg, C. Turner, Generation of Superhydrophobic Paper Surfaces by a Rapidly Expanding Supercritical Carbon Dioxide-Alkyl Ketene Dimer Solution, J. Supercrit. Fluids 49 (1) (2009) 117–124, https://doi.org/10.1016/J.SUPFLU.2008.11.015.

[31] P. Olin, C. Hyll, L. Ovaskainen, M. Ruda, O. Schmidt, C. Turner, L. Wågberg, Development of a Semicontinuous Spray Process for the Production of Superhydrophobic Coatings from Supercritical Carbon Dioxide Solutions, Ind. Eng. Chem. Res. 54 (3) (2015) 1059–1067, https://doi.org/10.1021/IE503798K/SUPPL_FILE/IE503798K_SI_001.PDF.

[32] O. Werner, C. Turner, Investigation of Different Particle Sizes on Superhydrophobic Surfaces Made by Rapid Expansion of Supercritical Solution with in Situ Laser Diffraction (RESS-LD), J. Supercrit. Fluids (2012) 67, https://doi.org/10.1016/j.supflu.2012.03.008.

[33] M.O. Gallyamov, L.N. Nikitin, A.Y. Nikolaev, A.N. Obraztsov, V.M. Bouznik, A. R. Khokhlov, Formation of Superhydrophobic Surfaces by the Deposition of Coatings from Supercritical Carbon Dioxide, Colloid J. 69 (4) (2007) 411–424, https://doi.org/10.1134/S1061933X07040035/METRICS.

[34] A. Pendurthi, S. Movafaghi, W. Wang, S. Shadman, A.P. Yalin, A.K. Kota, Fabrication of Nanostructured Omniphobic and Superomniphobic Surfaces with Inexpensive CO2 Laser Engraver, ACS Appl. Mater. Interfaces 9 (31) (2017) 25656–25661, https://doi.org/10.1021/ACSAMI.7B06924/SUPPL_FILE/AM7B06924_SI_006.AVI.

[35] Y.L. Zhan, M. Ruan, W. Li, H. Li, L.Y. Hu, F.M. Ma, Z.L. Yu, W. Feng, Fabrication of Anisotropic PTFE Superhydrophobic Surfaces Using Laser Microprocessing and Their Self-Cleaning and Anti-Icing Behavior, Colloids Surfaces A Physicochem. Eng. Asp. (2017) 535, https://doi.org/10.1016/j.colsurfa.2017.09.018.

[36] A. Anagnostopoulos, S. Knauer, Y. Ding, Y. Grosu, Giant Effect of Negative Compressibility in a Water-Porous Metal-CO2System for Sensing Applications, ACS Appl. Mater. Interfaces (2020), https://doi.org/10.1021/acsami.0c08752.

[37] Y. Li, Z. Zhang, B. Ge, X. Men, Q. Xue, One-Pot, Template-Free Synthesis of a Robust Superhydrophobic Polymer Monolith with an Adjustable Hierarchical Porous Structure, Green Chem. 18 (19) (2016) 5266–5272, https://doi.org/10.1039/C6GC01171C.

[38] W. Humphrey, A. Dalke, K. Schulten, VMD: Visual Molecular Dynamics, J. Mol. Graph. 14 (1) (1996) 33–38, https://doi.org/10.1016/0263-7855(96)00018-5.

[39] M. Lundgren, N.L. Allan, T. Cosgrove, N. George, Molecular Dynamics Study of Wetting of a Pillar Surface, Langmuir 19 (17) (2003) 7127–7129, https://doi.org/10.1021/la034224h.

[40] S. Khan, J.K. Singh, Wetting Transition of Nanodroplets of Water on Textured Surfaces: A Molecular Dynamics Study, Mol. Simul. 40 (6) (2014) 458–468, https://doi.org/10.1080/08927022.2013.819578.

[41] R.-A. Mitran, D. Lincu, L. Buhălţeanu, D. Berger, C. Matei, Shape-Stabilized Phase Change Materials Using Molten NaNO3 – KNO3 Eutectic and Mesoporous Silica Matrices, Sol. Energy Mater. Sol. Cells 215 (2020), 110644, https://doi.org/10.1016/j.solmat.2020.110644.

[42] A. Giacomello, C.M. Casciola, Y. Grosu, S. Meloni, Liquid Intrusion in and Extrusion from Non-Wettable Nanopores for Technological Applications, Eur. Phys. J. B 94 (8) (2021) 163, https://doi.org/10.1140/EPJB/S10051-021-00170-3.

[43] Y.G. Bushuev, Y. Grosu, M.A. Chorążewski, S. Meloni, Subnanometer Topological Tuning of the Liquid Intrusion/Extrusion Characteristics of Hydrophobic Micropores, Nano Lett. 22 (6) (2022) 2164–2169, https://doi.org/10.1021/acs.nanolett.1c02140.

[44] A. Anagnostopoulos, H. Navarro, A. Alexiadis, Y. Ding, Wettability of NaNO<inf>3</Inf> and KNO<inf>3</Inf> on MgO and Carbon Surfaces-Understanding the Substrate and the Length Scale Effects, J. Phys. Chem. C (2020) 124 (15), https://doi.org/10.1021/acs.jpcc.0c00978.

[45] M. Kanduč, Going beyond the Standard Line Tension: Size-Dependent Contact Angles of Water Nanodroplets, J. Chem. Phys. 147 (17) (2017), 174701, https://doi.org/10.1063/1.4990741.

[46] J. Zhang, P. Wang, M.K. Borg, J.M. Reese, D. Wen, A Critical Assessment of the Line Tension Determined by the Modified Young's Equation, Phys. Fluids 30 (8) (2018), 082003, https://doi.org/10.1063/1.5040574.
[47] T. Werder, J.H. Walther, R.L. Jaffe, T. Halicioglu, P. Koumoutsakos, On the Water−Carbon Interaction for Use in Molecular Dynamics Simulations of Graphite and Carbon Nanotubes, J. Phys. Chem. B 107 (6) (2003) 1345–1352, https://doi.org/10.1021/jp0268112.
[48] T. Koishi, K. Yasuoka, S. Fujikawa, X.C. Zeng, Measurement of Contact-Angle Hysteresis for Droplets on Nanopillared Surface and in the Cassie and Wenzel States: A Molecular Dynamics Simulation Study, ACS Nano 5 (9) (2011) 6834–6842, https://doi.org/10.1021/NN2005393/SUPPL_FILE/NN2005393_SI_002.PDF.
[49] J.V.L. Beckers, C.P. Lowe, S.W. De Leeuw, An Iterative PPPM Method for Simulating Coulombic Systems on Distributed Memory Parallel Computers, Mol. Simul. 20 (6) (1998) 369–383, https://doi.org/10.1080/08927029808022044.
[50] J. Lv, M. Bai, W. Cui, X. Li, The Molecular Dynamic Simulation on Impact and Friction Characters of Nanofluids with Many Nanoparticles System, Nanoscale Res. Lett. 6 (1) (2011) 1–8, https://doi.org/10.1186/1556-276X-6-200/FIGURES/6.
[51] N.A. Dhas, C.P. Raj, A. Gedanken, Synthesis, Characterization, and Properties of Metallic Copper Nanoparticles, Chem. Mater. 10 (5) (1998) 1446–1452, https://doi.org/10.1021/CM9708269.
[52] Vilaro, I.; Yagu, J. L.; Borro, S. Superhydrophobic Copper Surfaces with Anticorrosion Properties Fabricated by Solventless CVD Methods. **2017**. https://doi.org/10.1021/acsami.6b12119.
[53] Burkarter, E.; Saul, C. K.; Thomazi, F.; Cruz, N. C.; Zanata, S. M.; Roman, L. S.; Schreiner, W. H. Electrosprayed Superhydrophobic PTFE : A Non-Contaminating Surface. **2007**. https://doi.org/10.1088/0022-3727/40/24/027.
[54] S. Barthwal, S.H. Lim, Fabrication of Long-Term Stable Superoleophobic Surface Based on Copper Oxide/Cobalt Oxide with Micro-Nanoscale Hierarchical Roughness, Appl. Surf. Sci. 328 (2015) 296–305, https://doi.org/10.1016/J.APSUSC.2014.11.182.
[55] D. Quã, Rough Ideas on Wetting, Phys. A 313 (2002) 32–46.
[56] Shibuichi, S.; Onda, T.; Satoh, N.; Tsujii, K. Super Water-Repellent Surfaces Resulting from Fractal Structure. **1996**.
[57] P.A. Tran, T.J. Webster, Understanding the Wetting Properties of Nanostructured Selenium Coatings: The Role of Nanostructured Surface Roughness and Air-Pocket Formation, Int. J. Nanomedicine 2013 (2001) 8, https://doi.org/10.2147/IJN.S42970.
[58] M. Miwa, A. Nakajima, A. Fujishima, K. Hashimoto, T. Watanabe, Effects of the Surface Roughness on Sliding Angles of Water Droplets on Superhydrophobic Surfaces, Org. Coat. Appl. Polym. Sci. Proc 15 (2) (1999) 5754–5760, https://doi.org/10.1021/la991660o.
[59] C.R. Crick, I.P. Parkin, Water Droplet Bouncing—a Definition for Superhydrophobic Surfaces, Chem. Commun. 47 (44) (2011) 12059–12061, https://doi.org/10.1039/C1CC14749H.
[60] H. Yildirim Erbil, C. Elif Cansoy, Range of Applicability of the Wenzel and Cassie-Baxter Equations for Superhydrophobic Surfaces, Langmuir 25 (24) (2009) 14135–14145, https://doi.org/10.1021/LA902098A/SUPPL_FILE/LA902098A_SI_001.PDF.
[61] Gao, L.; Mccarthy, T. J. How Wenzel and Cassie Were Wrong. **2007**. https://doi.org/10.1021/la062634a.
[62] M.R.S. Shirazy, S. Blais, L.G. Fréchette, Mechanism of Wettability Transition in Copper Metal Foams: From Superhydrophilic to Hydrophobic, Appl. Surf. Sci. 258 (17) (2012), https://doi.org/10.1016/j.apsusc.2012.03.052.
[63] G. Wang, T.Y. Zhang, Oxygen Adsorption Induced Superhydrophilic-to-Superhydrophobic Transition on Hierarchical Nanostructured CuO Surface, J. Colloid Interface Sci. 377 (1) (2012), https://doi.org/10.1016/j.jcis.2012.03.035.
[64] R.G. Copperthwaite, P.R. Davies, M.A. Morris, M.W. Roberts, R.A. Ryder, The Reactive Chemisorption of Carbon Dioxide at Magnesium and Copper Surfaces at Low Temperature, Catal. Lett. 1 (1) (1988) 11–19, https://doi.org/10.1007/BF00765348.
[65] Deng, X.; Verdaguer, A.; Herranz, T.; Weis, C.; Bluhm, H.; Salmeron, M. Surface Chemistry of Cu in the Presence of CO 2 and H 2 O. https://doi.org/10.1021/la8011052.
[66] I. Nakamura, H. Nakano, T. Fujitani, T. Uchijima, J. Nakamura, Evidence for a Special Formate Species Adsorbed on the Cu–Zn Active Site for Methanol Synthesis, Surf. Sci. 402–404 (1998) 92–95, https://doi.org/10.1016/S0039-6028(97)00910-2.
[67] A. Kudo, S. Nakagawa, A. Tsuneto, T. Sakata, Electrochemical Reduction of High Pressure CO 2 on Ni Electrodes, J. Electrochem. Soc. (1993) 140 (6), https://doi.org/10.1149/1.2221599.
[68] L. Fan, K. Fujimoto, Fischer-Tropsch Synthesis in Supercritical Fluid: Characteristics and Application, Appl. Catal. A Gen. 186 (1–2) (1999), https://doi.org/10.1016/S0926-860X(99)00153-2.
[69] M.B. Ross, P. De Luna, Y. Li, C.T. Dinh, D. Kim, P. Yang, E.H. Sargent, Designing Materials for Electrochemical Carbon Dioxide Recycling, Nat. Catal. (2019), https://doi.org/10.1038/s41929-019-0306-7.
[70] Y. Yang, C.A. Mims, D.H. Mei, C.H.F. Peden, C.T. Campbell, Mechanistic Studies of Methanol Synthesis over Cu from CO/CO 2/H2/H2O Mixtures: The Source of C in Methanol and the Role of Water, J. Catal. (2013) 298, https://doi.org/10.1016/j.jcat.2012.10.028.
[71] T. Fujitani, I. Nakamura, T. Uchijima, J. Nakamura, The Kinetics and Mechanism of Methanol Synthesis by Hydrogenation of CO2 over a Zn-Deposited Cu(111) Surface, Surf. Sci. 383 (2–3) (1997), https://doi.org/10.1016/S0039-6028(97)00192-1.
[72] Y.F. Zhao, Y. Yang, C. Mims, C.H.F. Peden, J. Li, D. Mei, Insight into Methanol Synthesis from CO2 Hydrogenation on Cu(1 1 1): Complex Reaction Network and the Effects of H2O, J. Catal. 281 (2) (2011), https://doi.org/10.1016/j.jcat.2011.04.012.
[73] J. Toyir, P. Ramírez De La Piscina, J.L.G. Fierro, N. Homs, Highly Effective Conversion of CO2 to Methanol over Supported and Promoted Copper-Based Catalysts: Influence of Support and Promoter, Appl. Catal. B Environ. 29 (3) (2001), https://doi.org/10.1016/S0926-3373(00)00205-8.
[74] J. Díez-Ramírez, F. Dorado, A.R. De La Osa, J.L. Valverde, P. Sánchez, Hydrogenation of CO2 to Methanol at Atmospheric Pressure over Cu/ZnO Catalysts: Influence of the Calcination, Reduction, and Metal Loading, Ind. Eng. Chem. Res. 56 (8) (2017), https://doi.org/10.1021/acs.iecr.6b04662.
[75] Y. Yu, X. Dong, P. Chen, Q. Geng, H. Wang, J. Li, Y. Zhou, F. Dong, Synergistic Effect of Cu Single Atoms and Au-Cu Alloy Nanoparticles on TiO2for Efficient CO2Photoreduction, ACS Nano (2021), https://doi.org/10.1021/acsnano.1c03961.
[76] R. Dortwegt, E.V. Maughan, The Chemistry of Copper in Water and Related Studies Planned at the Advanced Photon Source, Proc. IEEE Part. Accel. Conf. 2 (2001) 1456–1458, https://doi.org/10.1109/pac.2001.986712.
[77] X. Su, H. Li, X. Lai, L. Zhang, X. Liao, J. Wang, Z. Chen, J. He, X. Zeng, Dual-Functional Superhydrophobic Textiles with Asymmetric Roll-Down/Pinned States for Water Droplet Transportation and Oil-Water Separation, ACS Appl. Mater. Interfaces 10 (4) (2018), https://doi.org/10.1021/acsami.7b15909.
[78] A.A. Alazab, T.A. Saleh, Magnetic Hydrophobic Cellulose-Modified Polyurethane Filter for Efficient Oil-Water Separation in a Complex Water Environment, J. Water Process Eng. (2022) 50, https://doi.org/10.1016/j.jwpe.2022.103125.
[79] H. Yu, M. Wu, G. Duan, X. Gong, One-Step Fabrication of Eco-Friendly Superhydrophobic Fabrics for High-Efficiency Oil/Water Separation and Oil Spill Cleanup, Nanoscale 14 (4) (2022), https://doi.org/10.1039/d1nr07111d.
[80] N. Wang, D. Xiong, Y. Deng, Y. Shi, K. Wang, Mechanically Robust Superhydrophobic Steel Surface with Anti-Icing, UV-Durability, and Corrosion Resistance Properties, ACS Appl. Mater. Interfaces 7 (11) (2015), https://doi.org/10.1021/acsami.5b00558.
[81] P. Varshney, S.S. Mohapatra, Durable and Regenerable Superhydrophobic Coatings for Brass Surfaces with Excellent Self-Cleaning and Anti-Fogging Properties Prepared by Immersion Technique, Tribol. Int. (2018) 123, https://doi.org/10.1016/j.triboint.2018.02.036.